crystals

MDPI

Article

Electrochemical Properties of Ultrathin $LiNi_{1/3}Mn_{1/3}Co_{1/3}O_2$ (NMC111) Slurry-Cast Li-Ion Battery

Byoung-Nam Park

Department of Materials Science and Engineering, Hongik University, 72-1, Sangsu-dong, Mapo-gu, Seoul 04066, Republic of Korea; metalpbn@hongik.ac.kr

Abstract: In thin $LiNi_{1/3}Mn_{1/3}Co_{1/3}O_2$ (NMC111) electrodes, pseudocapacitive behavior is notably enhanced due to their increased surface-to-volume ratio, which intensifies the role of the electrode–electrolyte interface. This behavior is driven by fast, reversible redox reactions and ion intercalation occurring near the surface, where the shorter diffusion path allows for more efficient ionic transport. The reduced thickness of the electrodes shortens the Li-ion diffusion distance, improving the diffusion coefficient by a factor of 40 compared to thicker electrodes, where ion transport is hindered by longer diffusion paths. The increased surface area and shorter diffusion paths promote faster electrochemical kinetics, allowing for quicker ion intercalation and deintercalation processes. The thin-film configuration enhances pseudocapacitive charge storage, which is essential for applications requiring rapid charge and discharge cycles. As a result, the combination of improved Li-ion diffusion and enhanced surface activity contributes to superior electrochemical performance, offering higher power densities, faster energy delivery, and better rate capability. This improvement in performance makes thin NMC111 electrodes particularly advantageous for applications such as high-power energy storage systems, where fast kinetics and high power densities are critical. These findings highlight the importance of interface engineering and material morphology in optimizing the performance of Li-ion batteries and similar electrochemical energy storage devices.

Keywords: Li-ion diffusivity; charge storage mechanism; NMC111; pseudocapacitance

Citation: Park, B.-N. Electrochemical Properties of Ultrathin $LiNi_{1/3}Mn_{1/3}Co_{1/3}O_2$ (NMC111) Slurry-Cast Li-Ion Battery. *Crystals* **2024**, *14*, 882. https://doi.org/10.3390/cryst14100882

Academic Editor: Weiqiang Lv

Received: 10 September 2024
Revised: 2 October 2024
Accepted: 8 October 2024
Published: 10 October 2024

1. Introduction

The rapid advancement of energy storage technologies is critical to meeting the growing demands for efficient, high-performance devices, particularly in sectors such as electric vehicles, renewable energy systems, and portable electronics. Lithium-ion batteries (LIBs) remain at the forefront of energy storage technologies due to their high energy density, long cycle life, and relatively low self-discharge rates [1–3]. However, achieving higher power densities and faster charge/discharge rates without compromising energy storage capacity remains a significant challenge. Addressing these limitations requires innovations in both material design and electrode architecture [4,5].

NMC111 oxides have garnered considerable attention as cathode materials in LIBs due to their favorable electrochemical properties, including high energy density, thermal stability, and tunable composition [6,7]. Despite these advantages, the performance of conventional NMC111 electrodes, particularly in thicker configurations, can be hindered by sluggish Li-ion diffusion and limited charge transfer kinetics [8–10]. Wang et al. reported an improved electrochemical model to study the effect of NMC111 electrode thickness on Li-ion battery performance, validated experimentally with electrode thicknesses from 31 to 130 μm [8]. The model shows minimal impact on cell utilization at low rates but decreasing performance with thicker electrodes and higher discharge rates (up to 5 C), mainly due to transport limitations and ohmic polarization, the latter being dominant at high C-rates. In thicker electrodes, Li-ion transport is restricted by the long diffusion paths, resulting in slower electrochemical reactions, reduced power capability, and inefficient charge storage.

Thin-film electrodes, on the other hand, offer a potential solution to these limitations. By reducing the electrode thickness, the surface area-to-volume ratio increases, allowing for more efficient interaction at the electrode–electrolyte interface [11,12]. This leads to enhanced pseudocapacitive behavior, characterized by fast, reversible redox reactions and ion intercalation processes at the surface or near-surface regions [13]. These processes significantly improve the kinetics of charge storage and transport, particularly in high-power applications. Moreover, the shorter diffusion paths in thin electrodes enable faster Li-ion transport, drastically increasing the diffusion coefficient compared to thicker electrodes [14,15]. This improvement in Li-ion mobility contributes to the superior rate capability and high power densities observed in thin-film NMC111 electrodes.

In addition to the enhanced pseudocapacitive behavior, the structural and surface properties of NMC111 thin films are critical in determining their electrochemical performance. The reduced thickness not only facilitates faster ion diffusion but also increases the influence of surface phenomena, which can be further tuned through interface engineering and material modifications. Understanding the mechanisms driving the improved electrochemical performance of thin NMC111 electrodes is essential for designing next-generation energy storage devices.

Beyond the comparison between thin and thick electrodes, it is critical to understand the role of the reaction front, specifically the electrode–electrolyte interface, in determining overall battery performance. This study investigates the impact of the reaction front by fabricating ultrathin NMC111 electrodes to explore their influence on pseudocapacitive behavior and Li-ion diffusion. By examining the interplay between thin-film morphology, interfacial characteristics, and electrochemical properties, this work provides key insights into the design of advanced NMC111 electrodes with enhanced power density, rapid charge/discharge capabilities, and superior energy storage performance. These findings contribute to the optimization of Li-ion battery materials for a wide range of applications, from high-power electronics to grid-scale energy storage systems.

2. Materials and Methods

2.1. Fabrication of Ultrathin and Thick NMC111 Slurry-Cast Electrodes

To refine the NMC111 powder (TOB, Xiamen, China), dry ball milling was performed for 6 h at a rotational speed of 400 rpm. For the slurry deposition process, a mixture was prepared using NMC111 as the active material, Carbon Black (CB), polyvinylidene fluoride (PVDF), and N-methyl-2-pyrrolidone (NMP) in a mass ratio of 8:1:1:30. Initially, PVDF and NMP were stirred at room temperature for 1 h to achieve homogeneity, after which the NMC111 and CB powders were introduced and thoroughly ground to ensure uniform dispersion.

The resulting slurry was carefully applied onto a 10 μm thick stainless steel (SS) foil with a 15 mm diameter using a precision applicator. This process ensured a consistent, uniform coating across the substrate. The coated foil was then dried overnight at 80 °C under vacuum conditions to remove any residual solvent and ensure complete adhesion of the electrode materials.

For the thin NMC111 electrode, the loading amount of the active material was controlled at 0.6 mg, corresponding to an approximate film thickness of ~100 nm. In contrast, the thick electrode configuration involved a loading of 3.0 mg, yielding a film thickness of ~5 μm. These specific loading conditions were tailored to optimize electrochemical performance and ensure consistency across different electrode thicknesses, providing a systematic comparison of their impact on battery behavior and performance metrics.

2.2. Electrochemical and Structural Characterizations

The slurry-deposited NMC111 electrodes were assembled into half-cells to evaluate their electrochemical performance. CR2032 coin cells were fabricated, utilizing Li metal as both the reference and counter electrodes, with the NMC111-coated electrode serving as the working electrode. The electrolyte employed was 1 M LiPF6 (Sigma Aldrich), dissolved in

a 1:1 volume ratio mixture of ethylene carbonate (EC) and diethyl carbonate (DEC), chosen for its favorable ionic conductivity and stability. Following assembly, the coin cells were allowed to equilibrate in an argon-filled glove box for 24 h to ensure proper electrolyte infiltration and electrode stabilization.

Electrochemical performance was rigorously tested, beginning with galvanostatic charge/discharge cycling. Specific capacity measurements were performed using a battery testing system (BTS, Neware) over a potential range of 3.0–4.3 V versus Li/Li^+. Charge and discharge cycles were conducted at current rates ranging from 1 C to 10 C, followed by a return to 1 C to evaluate the rate capability and long-term cycling stability of the electrodes. Cyclic voltammetry (CV) was carried out to further probe the redox behavior of the electrodes at scan rates of 0.1 mV/s, 0.3 mV/s, 0.5 mV/s, 0.8 mV/s, and 1.0 mV/s, within the same voltage window. For performance benchmarking, the theoretical capacity of NMC111 was assumed to be 145 mAh/g.

To complement the electrochemical measurements, structural characterization of the NMC111-deposited electrodes was performed. X-ray diffraction (XRD) was conducted on freshly fabricated electrodes to confirm phase purity and crystallographic alignment. Additionally, scanning electron microscopy (SEM) was used to capture high-resolution images of the electrode surface, providing insights into the microscopic morphology and the uniformity of the deposited layer.

2.3. Results and Discussion

Figure 1a shows the XRD pattern of the NMC111 electrode material. The distinct peaks in the diffraction pattern indicate the crystalline structure of the NMC111 material. These sharp peaks correspond to the specific lattice planes of the NMC111 crystal structure, confirming the formation of a well-ordered phase. The crystallite size of NMC111, determined using the Debye–Scherrer method, was measured to be 20 nm.

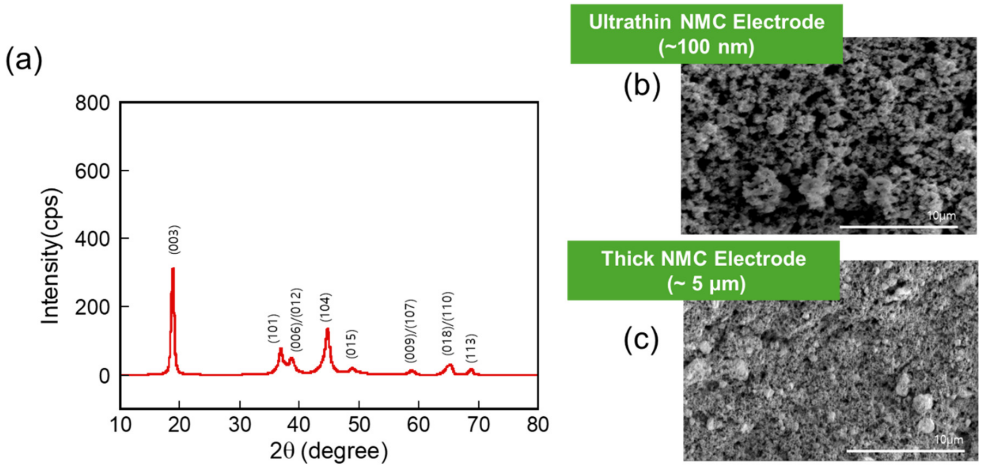

Figure 1. (**a**) X-ray diffraction (XRD) pattern of the NMC electrode deposited on Al foil. Scanning electron microscopy (SEM) images of the (**b**) ultrathin and (**c**) thick NMC111 electrodes on Al foil.

The SEM image in Figure 1b illustrates the surface morphology of an ultrathin NMC111 electrode with a thickness of approximately 100 nm. The image reveals a highly porous, nano-structured surface with a rough texture. The increased surface area due to the porous nature of the ultrathin film enhances electrochemical performance, as the surface interfaces play a significant role in pseudocapacitive charge storage and rapid ion transport. The scale bar indicates that the structural features are within the micrometer range, while the overall film thickness remains nanometric. The SEM image in Figure 1c shows the surface morphology of a thicker NMC111 electrode, approximately 5 μm in thickness. Compared to the ultrathin electrode, the thick electrode appears denser and less porous, with fewer surface features that can facilitate rapid ion diffusion. The compact structure of the thick

electrode increases the diffusion path length for Li ions, leading to slower electrochemical reactions and reduced overall performance. The image scale bar is again 10 µm, providing a sense of the surface structure and differences in porosity compared to the ultrathin sample.

The electrochemical performance of the NMC111 electrode was evaluated in coin cells using Li metal as both the counter and reference electrodes. CV was conducted at a scan rate of 0.1 mV/s over a potential window of 3.0 to 4.3 V versus Li/Li^+. Figure 2a shows the CV profiles, which exhibit a single pair of sharp anodic and cathodic peaks, corresponding to Li-ion de-intercalation and re-intercalation in the NMC111 structure. The redox peaks, observed at 3.8 V (oxidation) and 3.7 V (reduction), are attributed to the Ni^{2+}/Ni^{4+} redox couple, indicating stable Li cycling within the NMC lattice. The gradual stabilization of the peaks from the 1st to the 4th cycle suggests that the electrode material undergoes activation during the initial cycles and becomes more stable with further cycling. The overlapping curves in later cycles indicate good reversibility and stable electrochemical behavior, which are essential for long-term cycling performance in batteries.

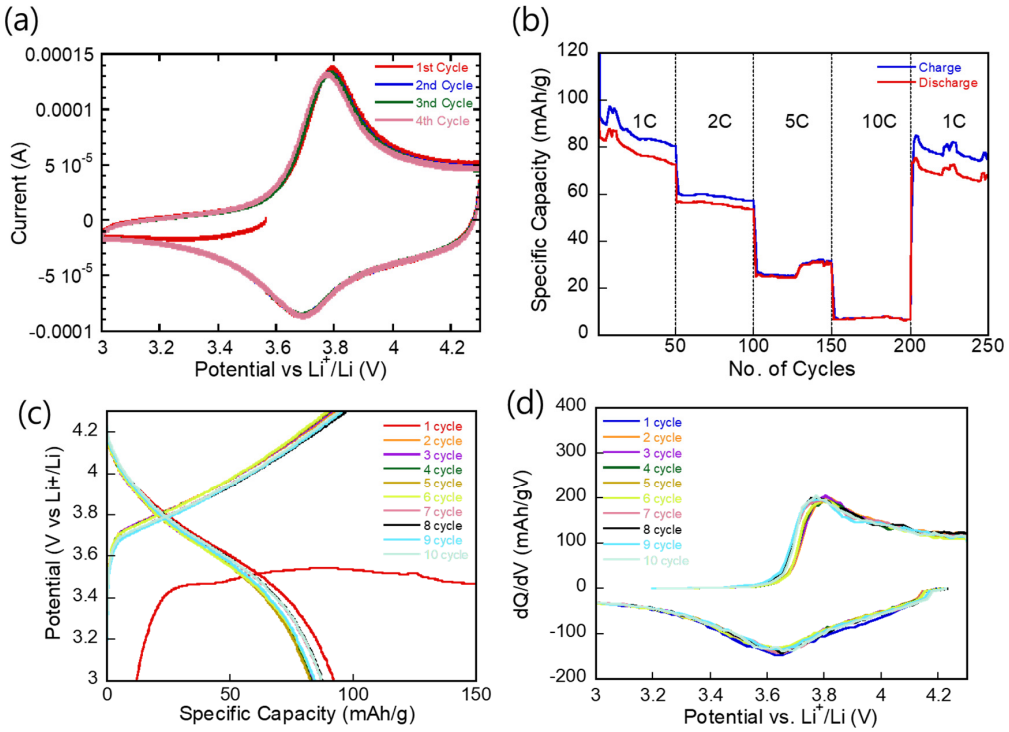

Figure 2. (**a**) Cyclic voltammetry (CV) curves at a scan rate of 0.1 mV/s, (**b**) rate capability, (**c**) charge/discharge potential profiles, and (**d**) differential capacity (dQ/dV) versus voltage plots for the ultrathin (~100 nm) NMC111 electrode in a Li-ion half-cell configuration.

Figure 2b exhibits high rate capability of NMC11 with blue representing charge and red representing discharge. The figure clearly demonstrates the rate-dependent capacity of the ultrathin NMC111 electrode. At lower rates (1 C and 2 C), the electrode delivers higher capacity, whereas at higher rates (5 C and 10 C), the capacity declines due to limited time for Li-ion diffusion. The electrode shows the ability to recover capacity when cycled at a slower rate (1 C) after experiencing high-rate cycling, indicating good structural resilience and reversibility of the material, despite the initial capacity fade. The closeness between the charge (blue) and discharge (red) curves at high C-rates suggests good coulombic efficiency, meaning that the electrode retains a significant portion of the stored charge during discharge, even though the overall capacity declines at higher rates.

The distinct plateaus, characteristic of phase transitions during the intercalation/deintercalation of Li ions, were not observed in the potential profile of Figure 2c. In many intercalation materials like NMC111, the distinct voltage plateaus are often a result of a

two-phase coexistence during the insertion or removal of Li ions. In ultrathin electrodes, this two-phase behavior may be less pronounced because of the small volume of the active material, leading to a more continuous change in voltage rather than the abrupt shifts seen in thicker electrodes where the two-phase coexistence can dominate.

Figure 2d shows the differential capacity versus voltage plot over multiple cycles (from 1 cycle to 10 cycles). The peaks in this plot correspond to the voltage at which phase transitions and redox reactions occur during Li-ion insertion and extraction. The relatively stable peak positions and intensities over several cycles reflect the good reversibility and consistency of the redox reactions in the ultrathin NMC electrode. The close alignment of the curves from cycle 1 to cycle 10 indicates excellent cycling stability and retention of electrochemical activity over time.

Rate-dependent CV measurements were performed to distinguish between diffusion-controlled and capacitive charge storage mechanisms. The cycling performance and rate capability of the NMC111 electrode are influenced by the balance between diffusion-controlled and surface capacitive behaviors. Diffusion-controlled storage, governed by the Li-ion diffusion within the electrode, is typically the rate-limiting step, whereas surface capacitive contributions, including both faradaic (surface redox reactions) and non-faradaic (electric double-layer formation) processes, are faster and enhance charge capacity at higher rates.

To quantify the contributions of these mechanisms, CV data (Figure 3a) were analyzed at different sweep rates using the power law equation $i = av^b$, where i is the current, v is the sweep rate, and a and b are adjustable parameters. This approach allowed us to differentiate the roles of diffusion-controlled, pseudocapacitive faradaic, and non-faradaic charge storage, providing insights into the overall charge storage behavior at varying rates. The b-values derived from the log i versus log v plot in Figure 3b indicate the dominant charge storage mechanism. A b-value of 0.5 suggests diffusion-controlled processes, while a b-value of 1.0 corresponds to surface capacitive behavior. For the NMC111 electrode, b-values of 0.70 (oxidation) and 0.77 (reduction) confirm that pseudocapacitive contributions dominate the charge storage process.

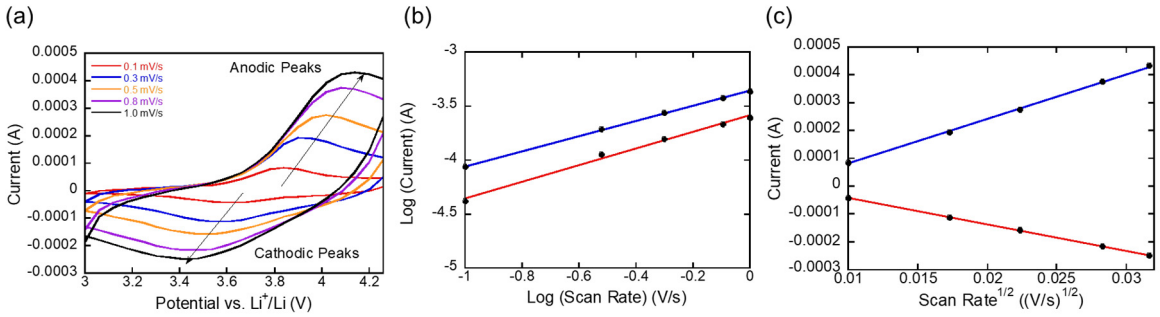

Figure 3. (**a**) Scan rate-dependent CV curves, (**b**) logarithmic plots of current versus scan rate for b-value calculation, and (**c**) peak current as a function of the square root of the scan rate for determining the Li-ion diffusion coefficient in the ultrathin (~100 nm) NMC111 electrode. The calculated b-values were 0.70 (anodic) and 0.77 (cathodic), and the diffusion coefficient was 1.6×10^{-8} cm^2/s.

The diffusion coefficient of Li ions was estimated using CV data at various scan rates, analyzed through the Randles–Sevcik equation:

$$I_p = 0.4463nFAC_{Li}\left(\frac{nF\nu D_{Li}}{RT}\right)^{\frac{1}{2}}$$

where I_p is the peak current, n the number of electrons transferred, F the Faraday constant (96,485 C·mol^{-1}), C_{Li} the initial concentration of Li^+ ions, A the electrode surface area, D_{Li} the diffusion coefficient, R the gas constant, and T the temperature. By plotting I_p against $v^{1/2}$, the diffusion coefficient was calculated as 1.6×10^{-8} cm^2·s^{-1} indicating efficient

Li-ion transport in the NMC111 electrode. This high diffusion coefficient underscores the superior electrochemical performance, particularly under high charge/discharge rates.

The pseudocapacitive charge storage behavior of the ultrathin NMC111 electrode was compared with the diffusion-dominated behavior of the thick slurry-cast NMC111 electrode. As shown in Figure 4a–c, the slurry-cast thick electrode exhibited a predominant diffusive component, with a *b*-value of 0.58 (oxidation), closely aligning with the theoretical value of 0.5, indicative of diffusion-controlled charge storage. In contrast, the ultrathin NMC111 electrode exhibited a *b*-value of 0.70 (oxidation), reflecting a significant contribution from surface-driven pseudocapacitive processes. Additionally, the Li-ion diffusion coefficient in the thick electrode was significantly lower, at 4.4×10^{-10} $cm^2 \cdot s^{-1}$, compared to the much higher value of 1.6×10^{-8} $cm^2 \cdot s^{-1}$ in the ultrathin electrode. This highlights the superior ionic mobility within the ultrathin electrode, which enhances its capacity to sustain rapid charge/discharge cycles, essential for high-rate applications.

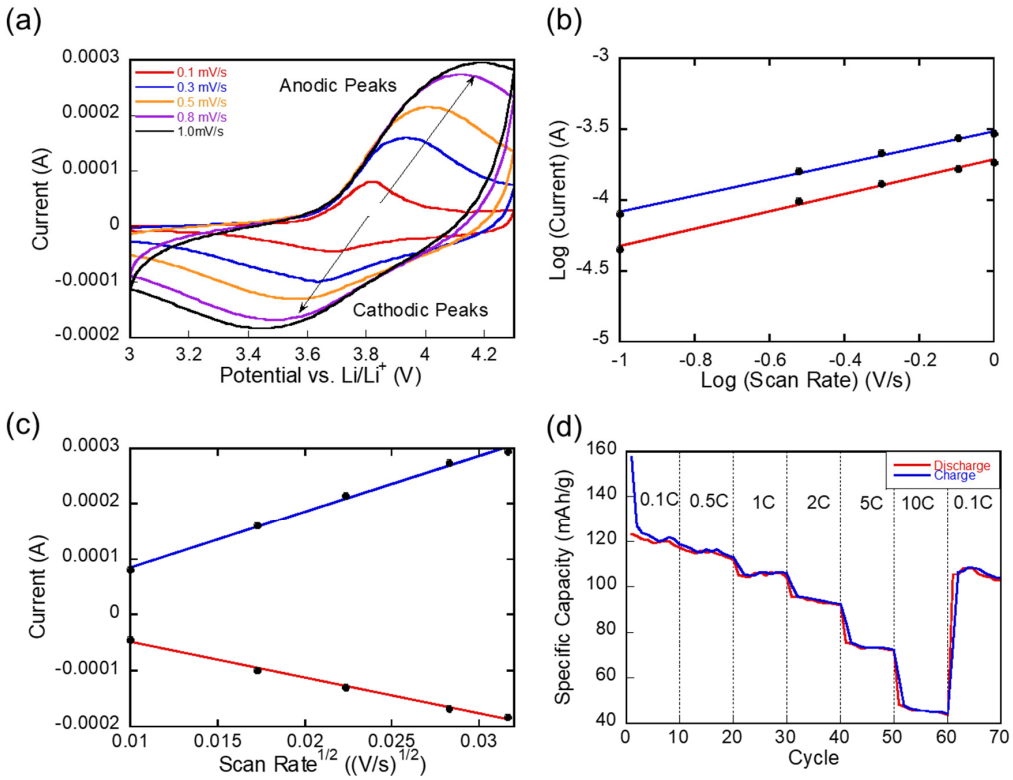

Figure 4. (**a**) Scan rate-dependent CV curves, (**b**) logarithmic plots of current versus scan rate for *b*-value calculation, and (**c**) peak current versus the square root of the scan rate for determining the Li-ion diffusion coefficient in the thick (~5 µm) NMC111 electrode. The calculated *b*-values were 0.58 (anodic) and 0.61 (cathodic), with a diffusion coefficient of 4.4×10^{-10} cm^2/s. (**d**) Rate capability plots of the thick NMC111 electrode.

The fundamental distinction between these two electrodes lies in their charge storage mechanisms. Pseudocapacitive materials, like the ultrathin NMC111 electrode, promote rapid surface redox reactions, leveraging a large accessible surface area, resulting in efficient but shallower ion interactions. This allows for faster kinetics, making such materials suitable for high-power applications. In contrast, diffusion-controlled materials, like the thick NMC111 electrode, support deeper ion penetration into the bulk of the material, which favors greater energy storage but at the cost of slower charge/discharge rates due to more limited ion diffusion. These findings demonstrate that optimizing electrode morphology and thickness is crucial for balancing pseudocapacitive and diffusion-controlled mechanisms, allowing tailored performance based on specific application requirements. While ultrathin electrodes are advantageous for fast-charging scenarios due to enhanced

surface reactions, thicker electrodes provide greater energy density but are constrained by slower ionic diffusion.

Despite the ultrathin NMC111 electrode's superior Li-ion diffusivity and dominant pseudocapacitive behavior, its specific charge capacity was significantly lower than that of the thick NMC111 electrode, as observed in Figures 2b and 4d. This might seem counterintuitive, given the enhanced kinetic parameters, such as faster Li-ion diffusion and a higher *b*-value, reflecting substantial pseudocapacitive contributions. While the ultrathin electrode demonstrates excellent rate capability due to rapid charge/discharge kinetics, its overall capacity is limited by surface-confined reactions, even at high C-rates, which restrict the full utilization of active material. In contrast, the thick NMC electrode, although characterized by slower kinetics, achieves greater specific capacity through deeper bulk intercalation of Li ions. The higher capacity at elevated C-rates in the thick electrode also suggests that the ultrathin electrode's increased surface area may facilitate more side reactions at the electrode–electrolyte interface, leading to capacity degradation that offsets its kinetic benefits.

The impedance spectroscopy (EIS) data for the thin and thick NMC111 electrodes exhibit distinct differences, as shown in Figure 5, which can be explained by the variation in charge transfer resistance (R_{ct}). The high-frequency semicircle represents the cathode electrolyte interphase (CEI) resistance (R_{CEI}) and contact resistances. The mid-to-low frequency semicircle corresponds to the charge transfer resistance related to the electrochemical reaction occurring at the electrode–electrolyte interface. In the thin NMC111 electrode of Figure 5a, the EIS spectra show lower overall resistance (smaller semicircles), indicating that both the CEI and charge transfer resistances are minimized. This can be attributed to the thinner nature of the electrode, which results in shorter ion diffusion paths and more efficient electron transfer, thereby reducing the resistance to charge transfer. The reduced thickness also ensures that the entire electrode surface is more accessible to the electrolyte, leading to a more uniform and stable SEI layer, which further minimizes the CEI resistance. For the thicker NMC111 electrode of Figure 5b, the EIS spectra show larger semicircles, indicating increased charge transfer resistance and possibly higher CEI resistance. The increased charge transfer resistance can be attributed to the thicker electrode, which leads to longer diffusion paths for Li ions and electrons, resulting in slower kinetics for charge transfer across the electrode–electrolyte interface. Additionally, the thicker electrode may result in a more uneven or thicker CEI layer, which increases R_{CEI}. This happens due to the difficulty in uniformly wetting and penetrating the electrolyte through the entire electrode thickness, especially during initial cycling.

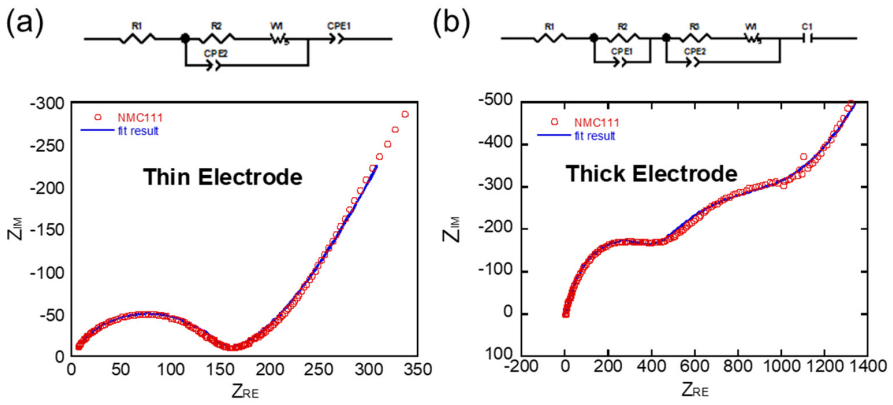

Figure 5. Nyquist plots from electrochemical impedance spectroscopy for the (**a**) ultrathin and (**b**) thick NMC111 electrodes. The charge transfer resistances were measured as 146 Ω and 588 Ω for the ultrathin and thick electrodes, respectively.

3. Conclusions

The pseudocapacitive behavior observed in thin NMC111 electrodes is related to the electrochemical processes that occur at or near the surface of the material. Pseudocapacitance refers to the charge storage mechanism where fast, reversible redox reactions take place at the electrode surface or within its near-surface region, involving ion adsorption and intercalation. In thin electrodes, such as thin films of NMC111, the surface area-to-volume ratio is higher, and the influence of interfaces (such as the electrode–electrolyte interface) becomes more significant. This enhances pseudocapacitive behavior because the charge storage can occur more quickly at the surface, allowing for faster kinetics of ion intercalation and deintercalation. Additionally, the short ion diffusion path in the thin electrode enables faster ionic transport. The improvement in the Li-ion diffusion coefficient by a factor of 40 in thin electrodes, compared to thicker electrodes, can be explained by the reduced diffusion distance that Li ions need to travel.

The higher capacity observed at elevated C-rates in the thick NMC111 electrode suggests that the ultrathin electrode's larger surface area, while beneficial for enhancing kinetics, may also contribute to increased side reactions at the electrode–electrolyte interface. These side reactions, such as electrolyte decomposition or formation of CEI, can consume active Li ions and degrade the electrode's capacity over time. As a result, despite the ultrathin electrode's enhanced Li-ion diffusivity and faster pseudocapacitive behavior, the occurrence of side reactions likely contributes to capacity losses, particularly under high-rate conditions. In contrast, the thick NMC111 electrode, with a smaller relative surface area, is less prone to such side reactions, allowing it to retain more active material for bulk intercalation, which compensates for its slower kinetics and results in higher overall capacity at elevated C-rates. This highlights the complex interplay between surface area, reaction mechanisms, and capacity retention, emphasizing the need to carefully balance surface area and bulk properties to optimize both rate capability and long-term stability in battery electrodes.

Funding: This research was supported by the Basic Science Research Program through the National Research Foundation of Korea (NRF) funded by the Ministry of Education (NRF-2015R1A6A1A03031833, and NRF-2020R1A2C1007258). This work was also supported by the 2024 Hongik Faculty Research Support Fund.

Data Availability Statement: Data is contained within the article.

Conflicts of Interest: The authors declare no conflict of interest.

References

1. Rajendran, S.; George, A.; Tang, Z.; Neumann, C.; Turchanin, A.; Arava, L.M.R. Regulating Li-Ion Transport through Ultrathin Molecular Membrane to Enable High-Performance All-Solid-State–Battery. *Small* **2023**, *19*, 2303625. [CrossRef]
2. Wang, Q.; Wang, S.; Lu, T.; Guan, L.; Hou, L.; Du, H.; Wei, H.; Liu, X.; Wei, Y.; Zhou, H. Ultrathin Solid Polymer Electrolyte Design for High-Performance Li Metal Batteries: A Perspective of Synthetic Chemistry. *Adv. Sci.* **2023**, *10*, 2205233. [CrossRef] [PubMed]
3. Quilty, C.D.; Wu, D.; Li, W.; Bock, D.C.; Wang, L.; Housel, L.M.; Abraham, A.; Takeuchi, K.J.; Marschilok, A.C.; Takeuchi, E.S. Electron and ion transport in lithium and lithium-ion battery negative and positive composite electrodes. *Chem. Rev.* **2023**, *123*, 1327–1363. [CrossRef] [PubMed]
4. Mahmood, N.; Tang, T.; Hou, Y. Nanostructured anode materials for lithium ion batteries: Progress, challenge and perspective. *Adv. Energy Mater.* **2016**, *6*, 1600374. [CrossRef]
5. Booth, S.G.; Nedoma, A.J.; Anthonisamy, N.N.; Baker, P.J.; Boston, R.; Bronstein, H.; Clarke, S.J.; Cussen, E.J.; Daramalla, V.; De Volder, M. Perspectives for next generation lithium-ion battery cathode materials. *APL Mater.* **2021**, *9*, 109201. [CrossRef]
6. Wagner, A.C.; Bohn, N.; Geßwein, H.; Neumann, M.; Osenberg, M.; Hilger, A.; Manke, I.; Schmidt, V.; Binder, J.R. Hierarchical structuring of NMC111-cathode materials in lithium-ion batteries: An in-depth study on the influence of primary and secondary particle sizes on electrochemical performance. *ACS Appl. Energy Mater.* **2020**, *3*, 12565–12574. [CrossRef]
7. Garcia, J.C.; Bareño, J.; Yan, J.; Chen, G.; Hauser, A.; Croy, J.R.; Iddir, H. Surface structure, morphology, and stability of Li $(Ni_{1/3}Mn_{1/3}Co_{1/3})O_2$ cathode material. *J. Phys. Chem. C* **2017**, *121*, 8290–8299. [CrossRef]
8. Xu, M.; Reichman, B.; Wang, X. Modeling the effect of electrode thickness on the performance of lithium-ion batteries with experimental validation. *Energy* **2019**, *186*, 115864. [CrossRef]

9. Arnot, D.J.; Mayilvahanan, K.S.; Hui, Z.; Takeuchi, K.J.; Marschilok, A.C.; Bock, D.C.; Wang, L.; West, A.C.; Takeuchi, E.S. Thick electrode design for facile electron and ion transport: Architectures, advanced characterization, and modeling. *Acc. Mater. Res.* **2022**, *3*, 472–483. [CrossRef]
10. Yang, X.; Doyle-Davis, K.; Gao, X.; Sun, X. Recent progress and perspectives on designing high-performance thick electrodes for all-solid-state lithium batteries. *ETransportation* **2022**, *11*, 100152. [CrossRef]
11. Hong, J.; Park, B. Additive-free Electrophoretic-deposited Ti_3AlC_2 MAX phase Li-ion battery anode. *Mater. Lett.* **2023**, *330*, 133227. [CrossRef]
12. Wei, D.; Haque, S.; Andrew, P.; Kivioja, J.; Ryhänen, T.; Pesquera, A.; Centeno, A.; Alonso, B.; Chuvilin, A.; Zurutuza, A. Ultrathin rechargeable all-solid-state batteries based on monolayer graphene. *J. Mater. Chem. A* **2013**, *1*, 3177–3181. [CrossRef]
13. Zheng, H.; Li, J.; Song, X.; Liu, G.; Battaglia, V.S. A comprehensive understanding of electrode thickness effects on the electrochemical performances of Li-ion battery cathodes. *Electrochim. Acta* **2012**, *71*, 258–265. [CrossRef]
14. Mukherjee, R.; Krishnan, R.; Lu, T.-M.; Koratkar, N. Nanostructured electrodes for high-power lithium ion batteries. *Nano Energy* **2012**, *1*, 518–533. [CrossRef]
15. Lee, J.; Park, B.-N. Inducing and Understanding Pseudocapacitive Behavior in an Electrophoretically Deposited Lithium Iron Phosphate Li-Metal Battery as an Electrochemical Test Platform. *J. Phys. Chem. Lett.* **2024**, *15*, 7095–7102. [CrossRef] [PubMed]